Islamic University Journal of Applied Sciences (IUJAS)
https://journals.iu.edu.sa/jesc

Volume VIII, Issue II, December 2026, Pages 261-280

A Comparative Theoretical Study on Gamma-Ray Shielding Parameters of Organic NLO Compounds within the 0.1 MeV–20 MeV Energy Range Utilizing Multiple Modeling and Simulation Tools

M.A. Ahlam[1]*,

[1] Department of Physics, College of Science, Qassim University, Buraydah 51452, Saudi Arabia
*Corresponding author: (M.A. Ahlam), *Email Address:* **ahl.ali@qu.edu.sa**

Abstract

In this study, a systematic theoretical and computational evaluation is performed to investigate the radiation-shielding efficiency of two organic non-linear optical (NLO) compounds: 3-[1-(2-phenylhydrazinylidene)ethyl]-2H-chromen-2-one ($C_{17}H_{14}N_2O_2$) and 4-nitrophenyl hydrazone ($C_{13}H_{11}N_3O_2$). The investigation was conducted across a broad photon energy spectrum (0.1 MeV to 20 MeV) using a multi-platform simulation to ensure the highest degree of precision and reliability. Specifically, the shielding effectiveness was estimated by Monte Carlo simulations in Geant4, and the results were validated against computational tools including EpiXS, XCOM and Phy-X/PSD. Computational modeling and simulation effectively streamline candidate selection for specific shielding applications, serving as a time and cost-efficient alternative to laboratory experiments. Fundamental parameters, including the mass attenuation coefficient (μ_m), total atomic and electronic cross-section ($\sigma_{t,a}, \sigma_{t,el}$), effective atomic number (Z_{eff}), effective electron density (N_{eff}) and molar extinction coefficients (ε) were theoretically determined. The results demonstrate a high degree of agreement between the Monte Carlo- based predictions and the theoretical frameworks. Furthermore, these findings confirm that the investigated NLO compounds are promising, cost-effective candidates for advanced radiation-shielding applications.

Keywords: Organic NLO Material; Geant4 (Monte Carlo Simulation); Radiation Attenuation; Mass Attenuation Coefficient.

https://doi.org/10.63070/jesc.2026.043
Received 19 April 2026; Revised 23 September 2026; Accepted 26 September 2026.
Available online 30 September 2026.
Published by Islamic University of Madinah on behalf of *Islamic University Journal of Applied Sciences.*
This is a free open access article published under the Creative Commons Attribution 4.0 International license (CC BY 4.0): https://creativecommons.org/licenses/by/4.0/

1. Introduction

Nonlinear optical (NLO) materials are highly important due to their wide use in electronics and optoelectronics, with prominent applications including optical communications, lasers, optical switching, data storage, and radiation sensing [1-7]. Among them, organic nonlinear optical materials are particularly preferred because their optical behavior originates at the molecular level. This molecular origin allows researchers to easily modify their chemical structures to achieve specific optical properties. Compared to inorganic alternatives, organic materials offer greater structural diversity and greater flexibility in tailoring their chemical structures and nonlinear optical properties. [8]. Furthermore, given the widespread use of ionizing radiation in medical, industrial, and nuclear fields, measuring radiation levels and material absorption is essential. This necessitates the evaluation of specific radiation interaction parameters, such as calculating the absorbed dose via photon transmission equations [5]. To study gamma-ray interactions with matter, a narrow-beam geometry setup based on the Beer–Lambert law is essential for accurately determining linear and mass attenuation coefficients [7]. The mass attenuation coefficient (μ_m) represents a fundamental parameter quantifying the probability of interaction between incident photons and a material's mass per unit area through scattering and absorption processes [9,10]. Calculating mass attenuation coefficients is critical for evaluating fundamental parameters of compounds or mixtures, including atomic and electronic cross-sections($\sigma_{t,a}$, $\sigma_{t,el}$), effective electron densities (N_{eff}), molar extinction coefficients (ε) and effective atomic numbers (Z_{eff}). Such parameters are essential in fields such as medical diagnostics, agricultural engineering, industrial radiography, and computed tomography, as well as in the core principles of nuclear shielding and radiation dosimetry. Numerous studies documented in the literature [11–31] have extensively investigated mass attenuation coefficients and radiation interaction parameters across a broad energy spectrum for a wide array of elements, compounds, and complex mixtures, using diverse theoretical, experimental, and analytical methodologies. Previous computational studies have utilized Monte Carlo simulations to evaluate the mass attenuation coefficients of various polymers across a range of photon energies [14,28]. Among the prominent theoretical developments, the XCOM computational framework was established to provide a robust method for determining attenuation parameters with high precision [32–34]. Subsequently, the transition of this tool to the Windows operating system was introduced by Gerward et al. [35], yielding the widely recognized software WinXCOM. In addition, extensive evaluations of the radiation interaction dynamics in diverse liquid and solid media have been performed [36], relying on the elemental data compiled by Hubbell and Seltzer [32] alongside Chantler [37]. In a related study [38], the energy-dependent behavior of the effective atomic number (Z_{eff}) was examined across common thermoluminescent dosimetric (TLD) materials (LiF, $CaCO_3$ and $CaSO_4$), establishing that (Z_{eff}) varies linearly with incident photon energy. In another investigation [39], empirical measurements of the mass attenuation coefficients for select TLD materials were conducted across various photon energies using a narrow-beam geometry coupled with a high-purity germanium detector. Motivated by the search for advanced alternatives, NLO materials hold significant potential for biological dosimetry applications, largely attributable to their mechanical strength, low mass density, economic

feasibility, and simple preparation methods. Numerous studies have extensively evaluated fundamental radiation interaction parameters across a broad photon energy range for various organic [1,4] and inorganic [6,7,9] nonlinear optical (NLO) materials. Specifically, evaluations of mass attenuation coefficients (μ_m) and effective atomic numbers (Z_{eff}) in organic NLO compounds indicated that their characteristically low (Z_{eff}) values make them highly applicable for radiation dosimetry [5]. Currently, the radiation interaction parameters for organic nonlinear optical (NLO) materials remain insufficiently documented, with no published data available for the two compounds under present study: 3-[1-(2-phenylhydrazinylidene)ethyl]-2H-chromen-2-one ($C_{17}H_{14}N_2O_2$) and 4-nitrophenyl hydrazone ($C_{13}H_{11}N_3O_2$). Therefore, this work conducts a comprehensive evaluation of their fundamental gamma-ray interaction parameters to fill this research gap. In this work, we present a detailed theoretical analysis of these parameters across a wide photon energy range from 0.1 MeV to 20 MeV. The parameters were systematically evaluated using comprehensive computational modeling. To ensure the reliability and precision of the results, a comparative analysis was performed using four internationally recognized computational tools: Geant4, EpiXS, XCOM, and Phy-X/PSD. This study demonstrates that the investigated organic NLO materials offer promising alternatives for biological dosimetry and related radiation applications.

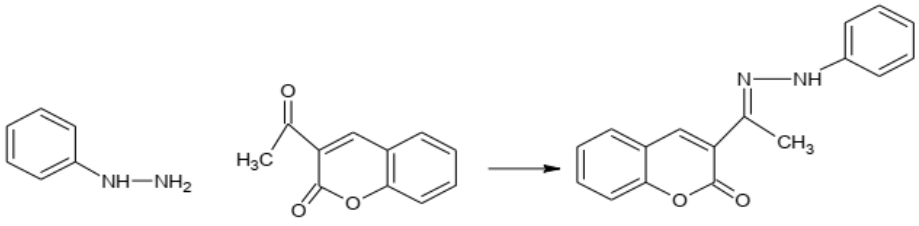
2. Investigated organic NLO compounds

2.1. 3-[1-(2-phenylhydrazinylidene)ethyl]-2H-chromen-2-one ($C_{17}H_{14}N_2O_2$)

This compound, commonly known as coumarin hydrazone, is an organic NLO crystal with a density of 1.30 g/cm³ that exhibits a needle-shaped morphology when grown via the slow evaporation technique. The grown crystal demonstrates high crystallinity and excellent optical transparency across the entire visible region, with an SHG efficiency 3.3 times higher than that of a standard KDP crystal. Furthermore, it maintains thermal stability up to 196°C, establishing it as a promising candidate for high-speed electro-optic and radiation-shielding applications.

Table 1. Atomic and weight fractions of elements in coumarin hydrazone.

Element	Atom Fraction	Weight Fraction
C (Carbon)	0.485714	0.733671
H (Hydrogen)	0.400000	0.050706
N (Nitrogen)	0.057143	0.100658
O (Oxygen)	0.057143	0.114965



Phenylhydrazine + 3-acetyl-2*H*-chromen-2-one → 3-[1-(2-phenylhydrazinylidene) ethyl]-2*H*-chromen-2-one

Fig.1. Schematic representation of coumarin hydrazone crystal synthesis.

2.2. 4-nitrophenyl hydrazone ($C_{13}H_{11}N_3O_2$)

This organic NLO crystal, with a density of 1.428 g/cm³, exhibits a needle-shaped morphology when prepared using the slow evaporation technique. The harvested crystal exhibits a high degree of crystallinity along with optical transparency throughout the entire visible spectrum. Furthermore, it exhibits significant thermal stability up to 146°C and an SHG efficiency 15.39 times higher than that of a standard KDP crystal, establishing it as a superior candidate for advanced nonlinear optical and radiation-shielding devices.

Table 2. Atomic and weight fractions of elements in 4-nitrophenyl hydrazone.

Element	Atom Fraction	Weight Fraction
C (Carbon)	0.448276	0.647225
H (Hydrogen)	0.379310	0.045961
N (Nitrogen)	0.103448	0.174180
O (Oxygen)	0.068966	0.132634

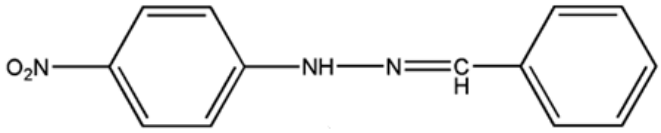


Fig. 2. Chemical structure of 4-nitrophenyl hydrazone $C_{13}H_{11}N_3O_2$ [44]

3. Calculation method

Mass Attenuation Coefficients (μ_m)

The mass attenuation coefficients were obtained for the investigated compounds using the photon transmission method. This fundamental radiation interaction process is described by the following mathematical expression [4,21,22,28]:

$$I = I_o \exp(-\mu_m t) \qquad (1)$$

In this expression, (I) and (I_o) denote the unattenuated and attenuated photon intensities respectively. The parameter (μ_m) represents the mass attenuation coefficient characteristic of the material, while (t) signifies the sample's mass thickness.

The mixture rule is employed to determine the total mass attenuation coefficient for any chemical compound or multi-elemental mixture. This principle calculates the overall attenuation as the weighted sum of the mass attenuation coefficients of its constituent elements, relative to their weight fractions.

$$\mu_m = \sum iW_i(\mu_m)_i \qquad (2)$$

In this context, (W_i) and $(\mu_m)_i$ denote the weight fraction and the mass attenuation coefficient of the i^{th} individual element within the medium, respectively. For chemical compounds, the weight fraction (W_i) is defined by the following mathematical relationship:

$$W_i = \frac{n_i\, A_i}{\sum_j n_j\, A_j} \qquad (3)$$

where (A_i) represents the atomic weight of the i^{th} element, (n_i) denotes the number of formula units, $(\sum_j n_j)$ signifies the total atom count in the molecular formula and (A_j) refers to the molecular weight of the j^{th} constituent element.

Effective Atomic Number $(\boldsymbol{Z_{eff}})$

The effective atomic number is calculated using the following equation:

$$Z_{eff} = \frac{\sigma_{t,a}}{\sigma_{t,el}} \qquad (4)$$

In this equation, $(\sigma_{t,a})$ and $(\sigma_{t,el})$ denote the total atomic and electronic cross-sections respectively. The total atomic cross-section is obtained from the following equation:

$$\sigma_{t,a} = \frac{1}{N_A} \frac{\mu_m}{\sum_i W_i/A_i} \qquad (5)$$

In this equation, (N_A) denotes Avogadro's number $(N_A = 6.02214 \times 10^{23})$. Furthermore, the total electronic cross-section $(\sigma_{t,el})$ is calculated through the following expression:

$$\sigma_{t,el} = \frac{1}{N_A} \sum_i \frac{f_i A_i}{Z_i} (\mu_m)_i \qquad (6)$$

In this expression, (f_i) denotes the fractional number of atoms for the i^{th} element, while (Z_i) denotes the atomic number of the corresponding element within the chemical compound or mixture.

Effective Electron Densities $(\boldsymbol{N_{eff}})$

The effective electron density is calculated using the following mathematical expression:

$$N_{eff} = \frac{\mu_m}{\sigma_{t,el}} = \frac{N_A}{M} Z_{eff} \sum_i n_i \qquad (7)$$

In this relation, (M/n) denotes the average atomic weight. Furthermore, $(\sum_i n_i = n)$ represents the total number of atoms in the molecular formula.

Molar Extinction Coefficient $(\boldsymbol{\varepsilon})$

The following expression was used to calculate the molar extinction coefficient:

$$\boldsymbol{\varepsilon} = \mathbf{0}.4343 \times N_A \times \sigma_{t,a} \qquad (8)$$

where, $(\sigma_{t,a})$ represents the total atomic cross-section.

4. Simulation methods

The radiation shielding effectiveness of two organic NLO compounds, $C_{17}H_{14}N_2O_2$ and $C_{13}H_{11}N_3O_2$, was investigated using Geant4 v11.1.1 Monte Carlo simulations over the photon energy range of 0.1 MeV–20 MeV. The simulations employed a monoenergetic, monodirectional pencil beam of 1,000,000 primary gamma photons per energy, directed perpendicular to the target samples. The FTFP_BERT_HP physics base was used with G4EmLivermorePhysics (G4-Liv) as the electromagnetic physics model. A narrow-beam, good-geometry configuration was employed, with

the photon source positioned 30 cm upstream of the sample and directed along the sample axis. The uncollided photon fraction was determined by counting the primary photons reaching the rear boundary of the sample without undergoing a physical interaction. Therefore, no additional downstream detector distance was required. The attenuation of gamma rays was determined from the ratio of the number of transmitted photons in the presence of the sample to the number of photons recorded without the sample [31,40]. A constant mass thickness of 0.15 g/cm^2 was used for all investigated photon energies. The corresponding physical thickness of each sample was calculated using the following equation:

$$t = \frac{0.15}{\rho} \qquad (9)$$

where t is the physical thickness in cm and ρ is the material density in g/cm³. Accordingly, the physical thicknesses were 0.1154 cm for $C_{17}H_{14}N_2O_2$, with a density of 1.300 g/cm^3, and 0.1050 cm for $C_{13}H_{11}N_3O_2$, with a density of 1.428 g/cm^3. For comparison, the calculated radiation-interaction and shielding parameters were compared with those obtained from three established theoretical platforms: EpiXS, based on the EPICS2017 and EPDL97 nuclear data libraries; XCOM, which uses the NIST photon cross-section database; and Phy-X/PSD, which provides photon-interaction data based on standard theoretical databases.

5. Results and discussion

In this work, the mass attenuation coefficients (μ_m) for the investigated organic NLO compounds were determined across a broad energy range (0.1 MeV–20 MeV) using the Geant4 Monte Carlo toolkit. To ensure the reliability of the simulation results, a rigorous cross-verification was performed by comparing the Geant4-derived data with theoretical values obtained from three established platforms: EpiXS, XCOM, and Phy-X/PSD. These computational tools provide comprehensive photon interaction data for diverse chemical compositions. Table 3 summarizes the calculated (μ_m) values for the studied samples and the percentage deviations (%Δ) between the Geant4 results and the three theoretical references, as defined by the following equations [28]:

$$\%\Delta_1 = 100 \times \left| \frac{\mu_{Epixs} - \mu_{G4}}{\mu_{Epixs}} \right| \qquad (10)$$

$$\%\Delta_2 = 100 \times \left| \frac{\mu_{\mathrm{XCOM}} - \mu_{G4}}{\mu_{\mathrm{XCOM}}} \right| \qquad (11)$$

$$\%\Delta_3 = 100 \times \left| \frac{\mu_{\mathrm{Phy-X/PSD}} - \mu_{G4}}{\mu_{\mathrm{Phy-X/PSD}}} \right| \qquad (12)$$

Table 3. Mass attenuation coefficients and corresponding percentage deviations between the Geant4 results and the three theoretical tools for the $C_{17}H_{14}N_2O_2$ and $C_{13}H_{11}N_3O_2$ organic NLO compounds over the selected gamma-ray energy range.

Gamma Energy (MeV)	Mass Attenuation Coefficient (μ_m (cm^2/g))													
	$C_{17}H_{14}N_2O_2$							$C_{13}H_{11}N_3O_2$						
	Geant4	EpiXS	%Δ_1	XCOM	%Δ_2	Phy-X/PSD	%Δ_3	Geant4	EpiXS	%Δ_1	XCOM	%Δ_2	Phy-X/PSD	%Δ_3
0.1	0.159 ± 0.0010	0.159	0.012	0.159	0.031	0.159	0.034	0.159 ± 0.0010	0.159	0.034	0.159	0.017	0.159	0.011

0.15	0.142 ± 0.0010	0.141	0.002	0.142	0.035	0.142	0.043	0.141 ± 0.0010	0.141	0.039	0.141	0.114	0.141	0.087
0.2	0.129 ± 0.0009	0.129	0.009	0.129	0.008	0.129	0.043	0.1285 ± 0.0009	0.129	0.061	0.129	0.086	0.129	0.096
0.3	0.112 ± 0.0009	0.112	0.092	0.112	0.125	0.112	0.129	0.111 ± 0.0009	0.112	0.054	0.112	0.069	0.112	0.092
0.4	0.100 ± 0.0008	0.100	0.069	0.100	0.170	0.100	0.126	0.100 ± 0.0008	0.100	0.046	0.100	0.103	0.100	0.105
0.5	0.091 ± 0.0008	0.091	0.019	0.092	0.097	0.092	0.094	0.091 ± 0.0008	0.091	0.025	0.091	0.104	0.091	0.099
0.6	0.0845 ± 0.0008	0.085	0.130	0.085	0.184	0.085	0.188	0.084 ± 0.0008	0.084	0.102	0.084	0.158	0.084	0.160
0.8	0.074 ± 0.0007	0.074	0.041	0.074	0.105	0.074	0.105	0.074 ± 0.0007	0.074	0.007	0.074	0.067	0.074	0.073
1	0.067 ± 0.0007	0.067	0.011	0.067	0.114	0.067	0.111	0.066 ± 0.0007	0.066	0.042	0.067	0.135	0.067	0.142
1.5	0.054 ± 0.0006	0.054	0.098	0.054	0.250	0.054	0.247	0.054 ± 0.0006	0.054	0.115	0.054	0.262	0.054	0.259
2	0.047 ± 0.0006	0.047	0.022	0.047	0.204	0.047	0.196	0.046 ± 0.0006	0.046	0.033	0.047	0.209	0.046	0.207
3	0.037 ± 0.0005	0.037	0.101	0.037	0.273	0.037	0.284	0.037 ± 0.0005	0.037	0.104	0.037	0.279	0.037	0.288
4	0.032 ± 0.0005	0.032	0.079	0.032	0.310	0.032	0.308	0.032 ± 0.0005	0.032	0.046	0.032	0.286	0.032	0.277
5	0.028 ± 0.0004	0.028	0.058	0.028	0.293	0.028	0.304	0.028 ± 0.0004	0.028	0.027	0.028	0.276	0.028	0.273
6	0.026 ± 0.0004	0.026	0.023	0.026	0.298	0.026	0.281	0.026 ± 0.0004	0.026	0.063	0.026	0.302	0.026	0.321
7	0.024 ± 0.0004	0.024	0.020	0.024	0.296	0.024	0.288	0.024 ± 0.0004	0.024	0.031	0.024	0.355	0.024	0.338
8	0.023 ± 0.0004	0.023	0.031	0.023	0.218	0.023	0.223	0.023 ± 0.0004	0.023	0.035	0.023	0.311	0.023	0.289
9	0.021 ± 0.0004	0.021	0.088	0.021	0.178	0.021	0.179	0.021 ± 0.0004	0.021	0.115	0.021	0.393	0.021	0.381
10	0.020 ± 0.0004	0.020	0.018	0.021	0.225	0.021	0.246	0.020 ± 0.0004	0.020	0.017	0.021	0.264	0.021	0.281
11	0.020 ± 0.0004	0.020	0.034	0.020	0.289	0.020	0.271	0.020 ± 0.0004	0.020	0.011	0.020	0.314	0.020	0.292
12	0.019 ± 0.0004	0.019	0.031	0.019	0.294	0.019	0.297	0.019 ± 0.0004	0.019	0.064	0.019	0.334	0.019	0.329
13	0.019 ± 0.0004	0.019	0.049	0.019	0.275	0.019	0.288	0.019 ± 0.0004	0.019	0.054	0.019	0.296	0.019	0.293
14	0.018 ± 0.0004	0.018	0.044	0.018	0.343	0.018	0.334	0.018 ± 0.0004	0.018	0.025	0.018	0.298	0.018	0.314
15	0.018 ± 0.0003	0.018	0.009	0.018	0.305	0.018	0.286	0.018 ± 0.0003	0.018	0.042	0.018	0.327	0.018	0.316
16	0.017 ± 0.0003	0.017	0.083	0.017	0.179	0.017	0.172	0.017 ± 0.0003	0.017	0.037	0.017	0.310	0.017	0.293
18	0.017 ± 0.0003	0.017	0.054	0.017	0.274	0.017	0.302	0.017 ± 0.0003	0.017	0.071	0.017	0.295	0.017	0.319
20	0.016 ± 0.0003	0.016	0.007	0.016	0.269	0.016	0.253	0.016 ± 0.0003	0.016	0.017	0.017	0.298	0.016	0.276

The comparison between the simulated and theoretical datasets of (μ_m) values versus photon energy for the investigated NLO crystals is presented in Figure 3, which reveals that the (μ_m) values decrease with increasing photon energy. This energy-dependent behavior is governed by the relative dominance of different photon interaction mechanisms. The variation of the mass attenuation coefficients with photon energy can be explained using the photoelectric effect, Compton scattering and pair production [7, 29, 41,42]. The energy dependence of the mass attenuation coefficients (μ_m) reveals three distinct energy regimes across the investigated spectrum: low, intermediate and high energy. In the low-energy region, a rapid and continuous drop in this parameter is observed uniformly for all NLO materials, where the photon-matter interaction is heavily dominated by the photoelectric effect, which exhibits a strong dependence on the atomic number (Z) of the constituent elements. Throughout the intermediate-energy spectrum, the (μ_m) values exhibit a gradual decrease with rising photon energy. This trend is

primarily attributed to the dominance of Compton scattering, where the interaction probability is mainly determined by the electron density of the NLO compounds rather than their atomic number. Alternatively, upon reaching the high-energy domain, the parameters display a subtle diminishing trend before transitioning into a steady, independent phase, which is a hallmark feature driven by the progression of pair-production events, which starts to contribute to the total attenuation cross-section at energies above 1.022 MeV and becomes more significant at higher energies, especially in multi-element organic compounds. Higher values of (μ_m) for the studied NLO compounds indicate superior radiation attenuation capabilities across the investigated photon energy range. As tabulated in Table 3, it is evident that the comparative analysis shows a degree of agreement between Geant4 and the theoretical codes (EpiXS, XCOM, and Phy-X/PSD). The percentage deviations ($\%\Delta_1, \%\Delta_2, \%\Delta_3$) remained remarkably low throughout the entire investigated energy spectrum. The small discrepancies observed between the Geant4 results and the theoretical values from EpiXS, XCOM, and Phy-X/PSD demonstrate good consistency among the computational approaches. These results support the use of Geant4 as a useful computational tool for investigating radiation-shielding parameters of organic nonlinear optical materials.

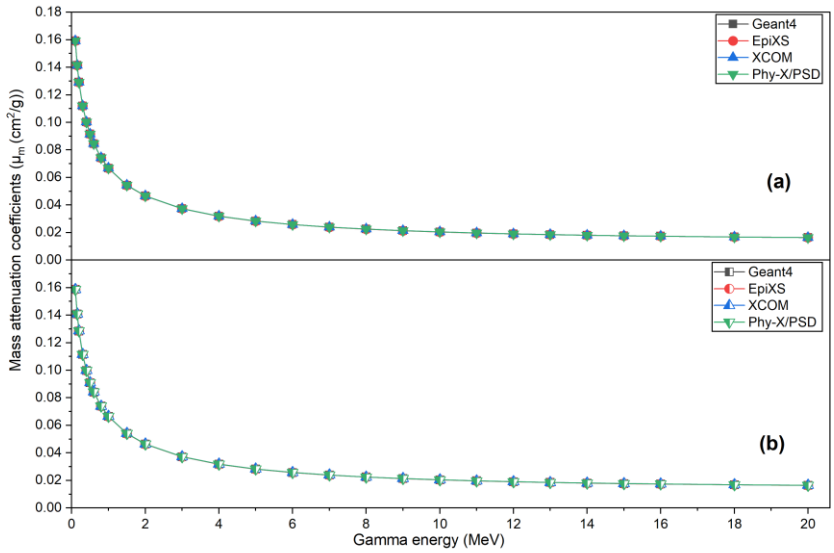


Fig.3. Comparative analysis of Geant4-simulated and theoretical mass attenuation coefficients for (a) $C_{17}H_{14}N_2O_2$ and (b) $C_{13}H_{11}N_3O_2$ organic NLO compounds over the selected gamma energy range.

The determined values of the total atomic cross-section ($\sigma_{t,a}$) and total electronic cross-section ($\sigma_{t,el}$) for the investigated organic NLO materials, calculated using (μ_m) are compiled in Tables 4 and 5, respectively. To show how they change with energy, plots of ($\sigma_{t,a}$) and ($\sigma_{t,el}$) against photon energy are presented in Figures 4 and 5. Across the studied energy spectrum, both cross-sectional parameters exhibit a physical trend that closely follows the behavior of the mass attenuation coefficient (μ_m)[5, 22].

Table 4. Total atomic cross section and corresponding percentage deviations between the Geant4 results and the three theoretical tools for the $C_{17}H_{14}N_2O_2$ and $C_{13}H_{11}N_3O_2$ organic NLO compounds over the selected gamma-ray energy range.

Gamma Energy (MeV)	Total atomic cross section ($\sigma_{t,a} \times 10^{-25}$ $(cm^2/atom)$)													
	$C_{17}H_{14}N_2O_2$							$C_{13}H_{11}N_3O_2$						
	Geant4	EpiXS	$\%\Delta_1$	XCOM	$\%\Delta_2$	Phy-X/PSD	$\%\Delta_3$	Geant4	EpiXS	$\%\Delta_1$	XCOM	$\%\Delta_2$	Phy-X/PSD	$\%\Delta_3$
0.1	21.015	21.017	0.010	21.021	0.031	21.021	0.032	21.927	21.919	0.036	21.923	0.017	21.924	0.013
0.15	18.677	18.677	0.004	18.684	0.035	18.685	0.041	19.456	19.463	0.037	19.478	0.113	19.472	0.085
0.2	17.045	17.047	0.007	17.047	0.008	17.052	0.041	17.750	17.760	0.059	17.765	0.086	17.766	0.093
0.3	14.770	14.784	0.090	14.789	0.125	14.789	0.127	15.392	15.400	0.052	15.403	0.069	15.406	0.089
0.4	13.221	13.230	0.067	13.244	0.170	13.238	0.123	13.775	13.781	0.044	13.789	0.103	13.789	0.102
0.5	12.073	12.075	0.017	12.085	0.097	12.084	0.092	12.574	12.577	0.023	12.587	0.103	12.587	0.097
0.6	11.153	11.167	0.128	11.173	0.184	11.174	0.186	11.620	11.632	0.100	11.638	0.158	11.638	0.158
0.8	9.802	9.806	0.039	9.812	0.105	9.812	0.103	10.213	10.213	0.005	10.220	0.067	10.220	0.071
1	8.812	8.813	0.009	8.822	0.114	8.821	0.109	9.175	9.179	0.040	9.188	0.135	9.188	0.140
1.5	7.163	7.169	0.096	7.181	0.250	7.180	0.245	7.459	7.468	0.112	7.479	0.262	7.479	0.257
2	6.147	6.149	0.020	6.160	0.204	6.159	0.193	6.403	6.405	0.030	6.417	0.209	6.416	0.205
3	4.922	4.927	0.099	4.936	0.273	4.936	0.282	5.130	5.135	0.102	5.144	0.279	5.145	0.286
4	4.207	4.210	0.077	4.220	0.310	4.220	0.306	4.389	4.391	0.044	4.401	0.286	4.401	0.274
5	3.736	3.739	0.056	3.747	0.293	3.748	0.302	3.900	3.901	0.025	3.911	0.276	3.911	0.271
6	3.404	3.405	0.020	3.415	0.298	3.414	0.279	3.553	3.555	0.060	3.564	0.302	3.565	0.319
7	3.157	3.156	0.022	3.166	0.296	3.166	0.286	3.297	3.298	0.028	3.308	0.355	3.308	0.336
8	2.968	2.968	0.033	2.975	0.218	2.975	0.221	3.101	3.102	0.033	3.111	0.311	3.110	0.286
9	2.819	2.817	0.090	2.824	0.178	2.824	0.177	2.943	2.947	0.113	2.955	0.393	2.954	0.379
10	2.696	2.695	0.020	2.702	0.225	2.702	0.244	2.820	2.821	0.015	2.828	0.264	2.828	0.278
11	2.595	2.594	0.036	2.603	0.289	2.602	0.268	2.717	2.717	0.013	2.726	0.314	2.725	0.290
12	2.511	2.511	0.029	2.518	0.294	2.518	0.295	2.630	2.631	0.061	2.638	0.334	2.638	0.326
13	2.440	2.441	0.047	2.447	0.275	2.447	0.285	2.558	2.559	0.052	2.565	0.296	2.565	0.291
14	2.379	2.380	0.042	2.387	0.343	2.387	0.332	2.496	2.496	0.023	2.503	0.298	2.503	0.311
15	2.329	2.329	0.007	2.336	0.305	2.335	0.284	2.443	2.444	0.040	2.451	0.327	2.450	0.314
16	2.287	2.285	0.085	2.291	0.179	2.291	0.170	2.398	2.398	0.035	2.405	0.310	2.405	0.290
18	2.211	2.212	0.052	2.217	0.274	2.218	0.300	2.322	2.324	0.069	2.329	0.295	2.330	0.317
20	2.156	2.156	0.009	2.162	0.269	2.161	0.250	2.266	2.266	0.014	2.272	0.298	2.272	0.273

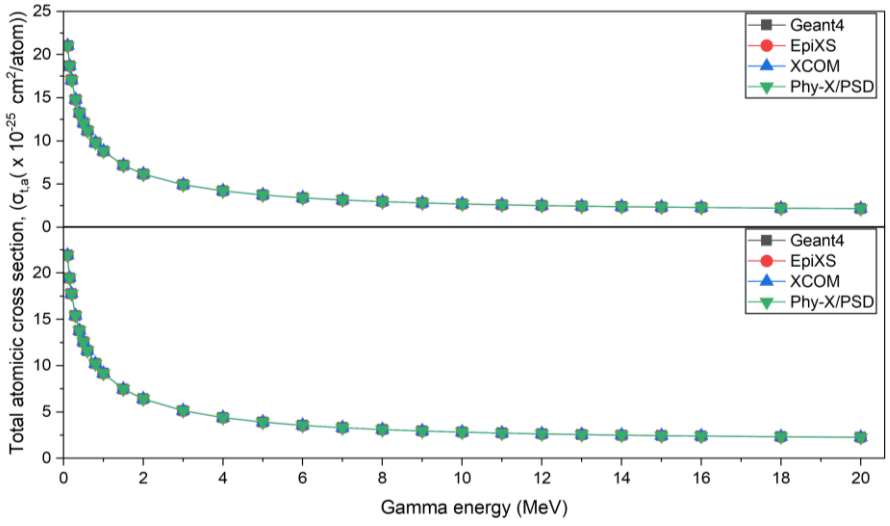


Fig.4. Comparative analysis of Geant4-simulated and theoretical total atomic cross section for (a) $C_{17}H_{14}N_2O_2$ and (b) $C_{13}H_{11}N_3O_2$ organic NLO compounds over the selected gamma energy range.

Table 5. Total electronic cross section and corresponding percentage deviations between the Geant4 results and the three theoretical tools for the $C_{17}H_{14}N_2O_2$ and $C_{13}H_{11}N_3O_2$ organic NLO compounds over the selected gamma-ray energy range.

Gamma Energy (MeV)	Total electronic cross section ($\sigma_{t,el} \times 10^{-25}$ $(cm^2/atom)$)													
	$C_{17}H_{14}N_2O_2$							$C_{13}H_{11}N_3O_2$						
	Geant4	EpiXS	$\%\Delta_1$	XCOM	$\%\Delta_2$	Phy-X/PSD	$\%\Delta_3$	Geant4	EpiXS	$\%\Delta_1$	XCOM	$\%\Delta_2$	Phy-X/PSD	$\%\Delta_3$
0.1	4.998	4.998	0.004	4.996	0.036	5.000	0.036	5.004	5.004	0.004	5.001	0.056	5.005	0.036
0.15	4.458	4.462	0.090	4.463	0.124	4.464	0.145	4.460	4.464	0.090	4.465	0.117	4.466	0.146
0.2	4.078	4.078	0.007	4.079	0.018	4.080	0.047	4.079	4.079	0.008	4.080	0.017	4.081	0.048
0.3	3.536	3.540	0.119	3.541	0.123	3.542	0.160	3.537	3.541	0.119	3.541	0.124	3.542	0.160
0.4	3.169	3.170	0.020	3.172	0.087	3.172	0.087	3.169	3.170	0.020	3.172	0.086	3.172	0.087
0.5	2.893	2.893	0.010	2.896	0.097	2.896	0.093	2.893	2.893	0.010	2.896	0.094	2.896	0.092
0.6	2.674	2.676	0.075	2.678	0.138	2.678	0.141	2.674	2.676	0.075	2.678	0.137	2.678	0.141
0.8	2.350	2.350	0.014	2.352	0.099	2.352	0.091	2.350	2.350	0.014	2.352	0.099	2.352	0.092
1	2.112	2.112	0.003	2.114	0.107	2.115	0.111	2.112	2.112	0.002	2.114	0.105	2.114	0.111
1.5	1.716	1.718	0.088	1.720	0.251	1.720	0.244	1.716	1.718	0.088	1.720	0.247	1.720	0.241
2	1.471	1.471	0.006	1.473	0.185	1.474	0.192	1.471	1.471	0.006	1.474	0.182	1.474	0.192
3	1.171	1.173	0.103	1.175	0.267	1.175	0.289	1.172	1.173	0.103	1.175	0.261	1.176	0.290
4	0.995	0.996	0.014	0.997	0.209	0.998	0.258	0.997	0.997	0.014	0.999	0.200	0.999	0.258
5	0.878	0.878	0.008	0.879	0.189	0.880	0.271	0.880	0.880	0.008	0.881	0.173	0.882	0.270
6	0.793	0.794	0.043	0.795	0.224	0.796	0.319	0.796	0.796	0.043	0.797	0.204	0.798	0.318
7	0.730	0.730	0.009	0.732	0.211	0.733	0.339	0.733	0.733	0.009	0.734	0.186	0.735	0.337
8	0.682	0.682	0.020	0.682	0.136	0.684	0.297	0.685	0.685	0.020	0.685	0.106	0.687	0.296
9	0.642	0.643	0.058	0.643	0.186	0.644	0.351	0.646	0.646	0.058	0.646	0.146	0.648	0.349
10	0.611	0.611	0.003	0.611	0.078	0.612	0.289	0.614	0.614	0.003	0.614	0.037	0.616	0.288
11	0.584	0.584	0.009	0.585	0.124	0.586	0.345	0.588	0.588	0.009	0.588	0.077	0.590	0.342
12	0.561	0.562	0.044	0.562	0.085	0.563	0.340	0.566	0.566	0.044	0.566	0.033	0.567	0.337
13	0.542	0.543	0.045	0.543	0.064	0.544	0.318	0.547	0.547	0.045	0.547	0.009	0.549	0.316
14	0.526	0.526	0.016	0.526	0.056	0.528	0.339	0.531	0.531	0.016	0.531	0.003	0.532	0.336
15	0.512	0.512	0.027	0.512	0.015	0.513	0.336	0.517	0.517	0.027	0.516	0.049	0.518	0.333
16	0.499	0.500	0.023	0.499	0.002	0.501	0.316	0.504	0.505	0.023	0.504	0.065	0.506	0.314
18	0.479	0.479	0.053	0.479	0.022	0.480	0.342	0.484	0.484	0.052	0.483	0.096	0.486	0.338
20	0.462	0.462	0.003	0.462	0.100	0.464	0.305	0.468	0.468	0.003	0.467	0.179	0.469	0.302

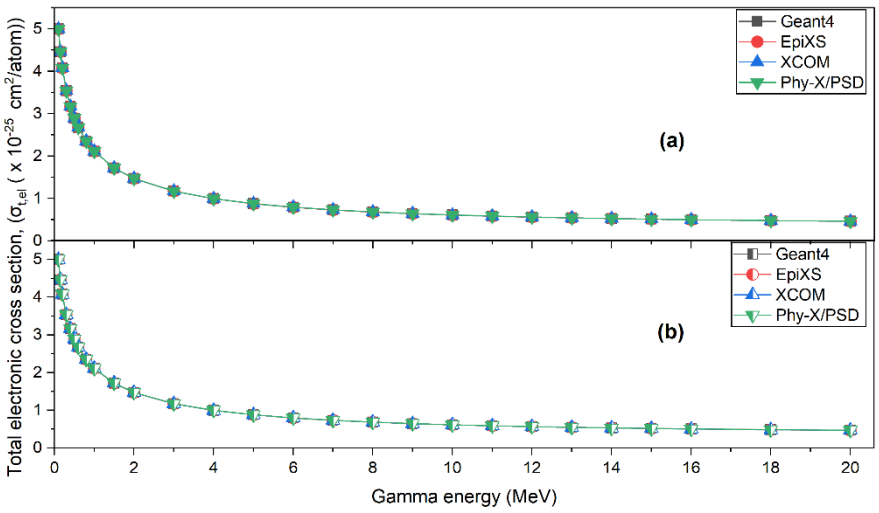


Fig.5. Comparative analysis of Geant4-simulated and theoretical total electronic cross section for (a) $C_{17}H_{14}N_2O_2$ and (b) $C_{13}H_{11}N_3O_2$ organic NLO compounds over the selected gamma energy range.

The mass attenuation coefficients (μ_m) derived from Geant4 simulations were utilized to determine the effective atomic numbers (Z_{eff}) and effective electron densities (N_{eff}) for the investigated organic NLO compounds via Eqs. (4) and (7). To validate the Geant4 simulation results, they were directly compared with the theoretical values obtained from EpiXS, XCOM, and Phy-X/PSD software. The detailed numerical results of (Z_{eff}) are tabulated in Table 6 for investigated samples.

Table 6. Effective atomic numbers and corresponding percentage deviations between the Geant4 results and the three theoretical tools for the $C_{17}H_{14}N_2O_2$ and $C_{13}H_{11}N_3O_2$ organic NLO compounds over the selected gamma-ray energy range.

Gamma Energy (MeV)	Effective atomic numbers (Z_{eff})													
	$C_{17}H_{14}N_2O_2$							$C_{13}H_{11}N_3O_2$						
	Geant4	EpiXS	$\%\Delta_1$	XCOM	$\%\Delta_2$	Phy-X/PSD	$\%\Delta_3$	Geant4	EpiXS	$\%\Delta_1$	XCOM	$\%\Delta_2$	Phy-X/PSD	$\%\Delta_3$
0.1	4.205 ± 0.028	4.205	0.006	4.208	0.067	4.205	0.004	4.382 ± 0.029	4.380	0.040	4.384	0.039	4.380	0.049
0.15	4.190 ± 0.030	4.186	0.094	4.186	0.088	4.185	0.104	4.362 ± 0.031	4.360	0.053	4.362	0.004	4.360	0.061
0.2	4.180 ± 0.031	4.180	0.000	4.180	0.010	4.180	0.007	4.352 ± 0.032	4.354	0.051	4.355	0.068	4.353	0.045
0.3	4.177 ± 0.033	4.176	0.029	4.177	0.002	4.176	0.033	4.352 ± 0.034	4.349	0.067	4.350	0.055	4.349	0.071
0.4	4.172 ± 0.035	4.174	0.047	4.176	0.083	4.174	0.037	4.347 ± 0.036	4.348	0.024	4.347	0.017	4.347	0.015
0.5	4.173 ± 0.036	4.174	0.006	4.173	0.000	4.173	0.001	4.347 ± 0.038	4.347	0.012	4.347	0.009	4.347	0.005
0.6	4.171 ± 0.038	4.173	0.053	4.173	0.046	4.173	0.045	4.345 ± 0.039	4.347	0.025	4.346	0.021	4.346	0.018
0.8	4.172 ± 0.040	4.173	0.025	4.172	0.006	4.172	0.012	4.347 ± 0.042	4.346	0.009	4.345	0.032	4.346	0.021
1	4.172 ± 0.042	4.173	0.012	4.172	0.006	4.172	0.002	4.344 ± 0.044	4.346	0.042	4.345	0.030	4.345	0.029
1.5	4.174 ± 0.048	4.174	0.007	4.174	0.001	4.174	0.001	4.346 ± 0.049	4.347	0.024	4.347	0.016	4.347	0.016
2	4.180 ± 0.051	4.181	0.015	4.181	0.019	4.180	0.002	4.353 ± 0.053	4.354	0.025	4.354	0.027	4.354	0.013
3	4.202 ± 0.057	4.202	0.004	4.202	0.006	4.202	0.007	4.376 ± 0.060	4.376	0.001	4.377	0.019	4.376	0.004
4	4.227 ± 0.062	4.229	0.062	4.231	0.101	4.229	0.048	4.403 ± 0.065	4.404	0.030	4.407	0.086	4.404	0.017
5	4.257 ± 0.067	4.259	0.047	4.262	0.103	4.258	0.031	4.434 ± 0.069	4.435	0.017	4.438	0.103	4.434	0.002
6	4.291 ± 0.070	4.290	0.022	4.295	0.074	4.290	0.041	4.466 ± 0.074	4.467	0.018	4.470	0.099	4.466	0.000
7	4.323 ± 0.073	4.322	0.031	4.327	0.085	4.321	0.053	4.498 ± 0.076	4.499	0.019	4.506	0.169	4.498	0.002
8	4.356 ± 0.077	4.353	0.053	4.359	0.082	4.352	0.077	4.530 ± 0.080	4.531	0.013	4.539	0.205	4.530	0.010
9	4.391 ± 0.079	4.384	0.148	4.390	0.008	4.383	0.174	4.560 ± 0.083	4.562	0.056	4.571	0.247	4.561	0.031
10	4.415 ± 0.082	4.414	0.017	4.422	0.147	4.413	0.046	4.592 ± 0.085	4.593	0.017	4.602	0.227	4.591	0.010
11	4.446 ± 0.081	4.444	0.045	4.453	0.165	4.442	0.077	4.623 ± 0.086	4.622	0.022	4.634	0.238	4.621	0.053
12	4.472 ± 0.085	4.472	0.015	4.482	0.209	4.470	0.045	4.650 ± 0.088	4.650	0.018	4.664	0.301	4.649	0.011
13	4.499 ± 0.087	4.499	0.001	4.508	0.211	4.497	0.033	4.677 ± 0.090	4.678	0.007	4.691	0.288	4.676	0.025
14	4.524 ± 0.089	4.525	0.026	4.537	0.287	4.523	0.007	4.704 ± 0.091	4.704	0.007	4.718	0.301	4.703	0.025
15	4.551 ± 0.089	4.550	0.020	4.564	0.290	4.548	0.053	4.729 ± 0.094	4.729	0.012	4.747	0.376	4.728	0.019
16	4.579 ± 0.090	4.574	0.108	4.587	0.176	4.572	0.147	4.753 ± 0.095	4.754	0.012	4.771	0.375	4.752	0.024
18	4.619	4.619	0.001	4.633	0.296	4.618	0.042	4.798	4.799	0.018	4.817	0.390	4.797	0.022

	± 0.092							± 0.097						
20	4.662 ± 0.095	4.661	0.012	4.679	0.368	4.659	0.055	4.841 ± 0.098	4.841	0.012	4.864	0.477	4.839	0.029

Figure 6 illustrates the variation of the effective atomic number $(\boldsymbol{Z_{eff}})$ for the investigated NLO material as a function of photon energy across a wide spectrum up to 20 MeV. A strong agreement is observed among the Geant4 simulation results and the theoretical predictions (EpiXS, XCOM, and Phy-X/PSD). At low photon energies (below 1 MeV), the $\boldsymbol{Z_{eff}}$ profile experiences a slight initial drop, which is governed by the shifting dominance from photoelectric absorption to Compton scattering. Crucially, beyond the 1.02 MeV threshold and up to 20 MeV, a continuous and monotonic increase in $\boldsymbol{Z_{eff}}$ is prominently observed. This ascending trend is physically attributed to the progressive dominance of the pair-production mechanism.

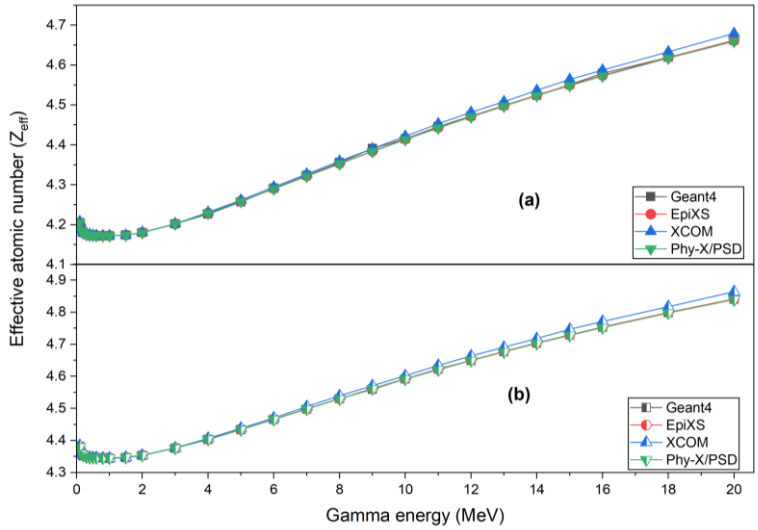


Fig.6 Comparative analysis of Geant4-simulated and theoretical effective atomic numbers for (a) $C_{17}H_{14}N_2O_2$ and (b) $C_{13}H_{11}N_3O_2$ organic NLO compounds over the selected gamma energy range.

Table 7 presents a comparative analysis of the calculated Z_{eff} values for the investigated organic NLO materials against various standard reference materials across the energy range of 122 keV to 1330 keV. The investigated compounds exhibit low Z_{eff} values ranging between 4.173 and 4.376, which are intrinsically attributed to their organic framework dominated by light elements (H, C, N, and O). Notably, these values are highly comparable to those of organic references and human muscle tissue, while remaining significantly lower than the inorganic counterparts such as KDP. Furthermore, the slight reduction in Z_{eff} as energy increases from 122 keV to 840 keV marks the physical transition from photoelectric absorption dominance to Compton scattering interactions. This strong equivalence to human tissue underscores the potential of these synthesized NLO crystals for biological radiation dosimetry and medical phantom applications.

Table 7. Effective atomic number (Z_{eff}) values of the investigated NLO materials as compared with those of organic and inorganic compounds, TLD materials, polymers, and human tissues.

E (KeV)	Effective atomic numbers (Z_{eff})											
	investigated NLO materials		Organic NLO materials[4]		inorganic NLO materials[7]		TLD materials[39]		Polymers [29]		Human tissues[43]	
	$C_{17}H_{14}N_2O_2$	$C_{13}H_{11}N_3O_2$	$C_6H_6N_2O_2$	$C_5H_5N_3O_2$	KDP	ADP	LiF	$CaCO_3$	POM	PAN	Bone	Muscle
122	4.207	4.376	4.698	4.829	9.614	5.453	6.054	9.825	4.022	4.066	5.996	3.435
356	4.177	4.351	4.651	4.776	9.216	5.170	6.006	10.005	4.011	4.052	6.004	3.434
511	4.175	4.348	4.635	4.757	9.225	4.989	5.987	10.051	4.005	4.046	5.901	3.437
662	4.173	4.344	4.625	4.755	8.906	4.468	5.988	10.052	4.002	4.042	5.994	3.435
840	4.173	4.343	4.615	4.734	8.957	4.014	6.001	10.041	3.999	4.039	6.024	3.446
1170	4.174	4.344	4.600	4.717	8.802	5.208	5.924	10.025	3.995	4.035	6.104	3.478
1275	4.175	4.345	4.597	4.713	8.894	4.676	6.002	10.037	3.994	4.033	6.199	3.517
1330	4.176	4.346	4.595	4.711	8.781	4.605	5.966	10.042	3.993	4.032	6.297	3.559

The comprehensive numerical values of the effective electron densities (N_{eff}) for the studied samples are systematically cataloged in Table 8.

Table 8. Effective electron densities and corresponding percentage deviations between the Geant4 results and the three theoretical tools for the $C_{17}H_{14}N_2O_2$ and $C_{13}H_{11}N_3O_2$ organic NLO compounds over the selected gamma-ray energy range.

Gamma Energy (MeV)	Effective electron densities (N_{eff} ($\times 10^{23}$ e^-/g))													
	$C_{17}H_{14}N_2O_2$							$C_{13}H_{11}N_3O_2$						
	Geant4	EpiXS	$\%\Delta_1$	XCOM	$\%\Delta_2$	Phy-X/PSD	$\%\Delta_3$	Geant4	EpiXS	$\%\Delta_1$	XCOM	$\%\Delta_2$	Phy-X/PSD	$\%\Delta_3$
0.1	3.184 ± 0.021	3.185	0.008	3.187	0.067	3.184	0.002	3.172 ± 0.021	3.171	0.038	3.173	0.039	3.171	0.047
0.15	3.173 ± 0.022	3.170	0.092	3.170	0.088	3.170	0.102	3.158 ± 0.022	3.156	0.051	3.158	0.004	3.156	0.059
0.2	3.166 ± 0.023	3.166	0.002	3.165	0.010	3.165	0.004	3.150 ± 0.023	3.152	0.053	3.152	0.068	3.152	0.048
0.3	3.163 ± 0.025	3.162	0.027	3.163	0.002	3.162	0.031	3.151 ± 0.025	3.149	0.065	3.149	0.055	3.148	0.068
0.4	3.160 ± 0.026	3.161	0.049	3.162	0.083	3.161	0.039	3.147 ± 0.026	3.147	0.026	3.147	0.017	3.147	0.017
0.5	3.161 ± 0.027	3.161	0.009	3.161	0.000	3.161	0.002	3.147 ± 0.027	3.147	0.015	3.147	0.009	3.147	0.007
0.6	3.159 ± 0.029	3.161	0.055	3.160	0.046	3.160	0.047	3.146 ± 0.029	3.147	0.027	3.146	0.021	3.146	0.020
0.8	3.159 ± 0.030	3.160	0.028	3.160	0.006	3.160	0.014	3.146 ± 0.030	3.146	0.007	3.145	0.032	3.146	0.019
1	3.160 ± 0.032	3.160	0.014	3.160	0.006	3.160	0.000	3.145 ± 0.032	3.146	0.044	3.146	0.030	3.146	0.031
1.5	3.161 ± 0.036	3.161	0.010	3.161	0.001	3.161	0.003	3.146 ± 0.035	3.147	0.026	3.147	0.016	3.147	0.018
2	3.166 ± 0.039	3.166	0.017	3.166	0.019	3.166	0.004	3.151 ± 0.038	3.152	0.027	3.152	0.027	3.152	0.015
3	3.182 ± 0.043	3.182	0.002	3.183	0.006	3.182	0.005	3.168 ± 0.043	3.168	0.001	3.169	0.019	3.168	0.002
4	3.201 ± 0.047	3.203	0.065	3.204	0.101	3.203	0.050	3.187 ± 0.047	3.188	0.032	3.190	0.086	3.188	0.019
5	3.224 ± 0.051	3.226	0.050	3.227	0.103	3.225	0.033	3.210 ± 0.050	3.210	0.019	3.213	0.103	3.210	0.004
6	3.250 ± 0.053	3.249	0.020	3.252	0.074	3.249	0.038	3.233 ± 0.053	3.233	0.020	3.236	0.099	3.233	0.003
7	3.274 ± 0.055	3.273	0.029	3.277	0.085	3.273	0.051	3.256 ± 0.055	3.257	0.022	3.262	0.169	3.256	0.001
8	3.299 ± 0.058	3.297	0.051	3.301	0.082	3.296	0.075	3.279 ± 0.058	3.280	0.015	3.286	0.205	3.279	0.008
9	3.325 ± 0.060	3.320	0.146	3.325	0.008	3.320	0.172	3.301 ± 0.060	3.303	0.058	3.309	0.247	3.302	0.033
10	3.344	3.343	0.015	3.349	0.147	3.342	0.044	3.324	3.325	0.019	3.332	0.227	3.324	0.008

	± 0.062							± 0.061						
11	3.367 ± 0.062	3.365	0.043	3.372	0.165	3.364	0.075	3.347 ± 0.062	3.346	0.020	3.355	0.238	3.345	0.050
12	3.387 ± 0.065	3.387	0.013	3.394	0.209	3.386	0.043	3.366 ± 0.064	3.366	0.020	3.376	0.301	3.366	0.009
13	3.4070 ± 0.066	3.407	0.003	3.414	0.211	3.406	0.030	3.386 ± 0.065	3.386	0.009	3.396	0.288	3.385	0.023
14	3.426 ± 0.068	3.427	0.028	3.436	0.287	3.426	0.005	3.405 ± 0.066	3.405	0.009	3.415	0.301	3.404	0.023
15	3.446 ± 0.067	3.446	0.018	3.457	0.290	3.445	0.050	3.423 ± 0.068	3.424	0.015	3.436	0.376	3.423	0.016
16	3.468 ± 0.068	3.464	0.106	3.474	0.176	3.463	0.144	3.441 ± 0.068	3.441	0.015	3.454	0.375	3.440	0.021
18	3.498 ± 0.069	3.499	0.002	3.509	0.296	3.497	0.040	3.474 ± 0.070	3.474	0.020	3.487	0.390	3.473	0.019
20	3.531 ± 0.072	3.530	0.010	3.544	0.368	3.529	0.053	3.504 ± 0.071	3.505	0.014	3.521	0.477	3.503	0.027

Figure 7 illustrates the energy-dependent behavior of the effective electron density (N_{eff}) for the synthesized organic NLO compounds within the energy range from 0.1 MeV to 20 MeV. Physically, the N_{eff} profile is directly proportional to the effective atomic number $\boldsymbol{Z_{eff}}$, which explains the similar physical trends observed between both parameters. Furthermore, a remarkable alignment is demonstrated between the Geant4 Monte Carlo simulation results and the validation benchmarks (EpiXS, XCOM, and Phy-X/PSD) across the entire spectrum.

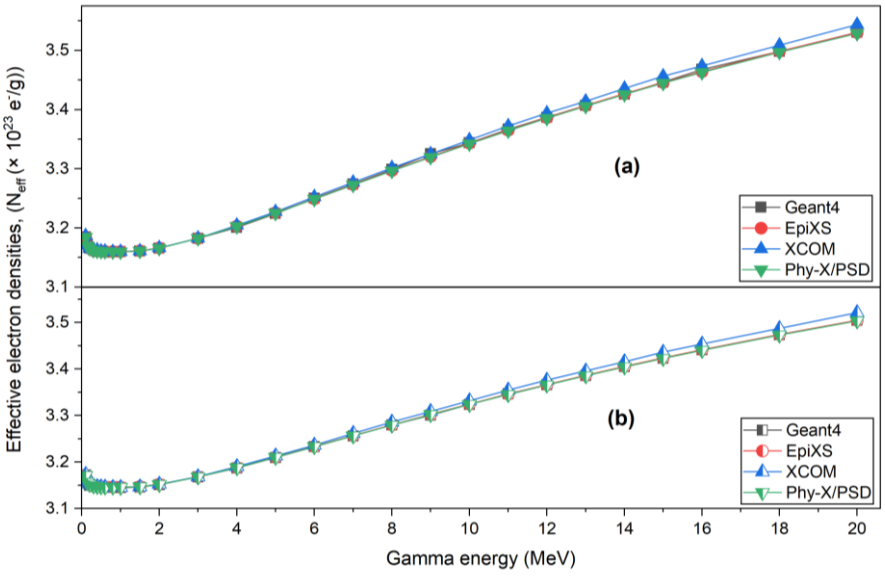


Fig.7. Comparative analysis of Geant4-simulated and theoretical effective electron densities for (a) $C_{17}H_{14}N_2O_2$ and (b) $C_{13}H_{11}N_3O_2$ organic NLO compounds over the selected gamma energy range

Figure 8 shows a direct linear relationship between ($\boldsymbol{Z_{eff}}$) and (N_{eff}) for the investigated organic NLO compounds across the energy range from 0.1 MeV to 20 MeV [7]. This highly linear trend is a natural physical consequence, as both parameters are governed by the same electron cloud of the material. Additionally, the $C_{13}H_{11}N_3O_2$ compound displays higher values than the $C_{17}H_{14}N_2O_2$ compound. This variation is attributable to their chemical structures; the $C_{13}H_{11}N_3O_2$ compound contains a higher proportion of heavier atoms (nitrogen and oxygen). This atomic composition increases the overall electron density, thereby enhancing the probability of radiation interactions within the material.

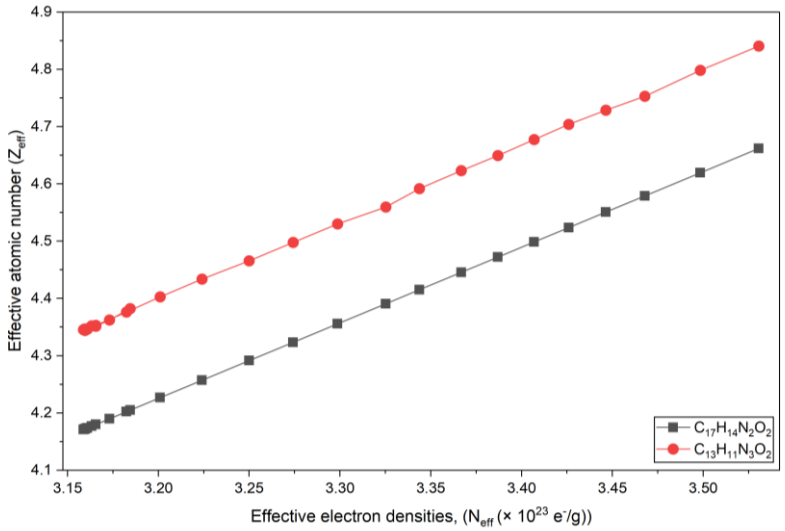


Fig. 8. Variation and correlation of $(\boldsymbol{Z_{eff}})$ and (N_{eff}) with photon energy for the investigated NLO compounds.

The molar extinction coefficients $(\boldsymbol{\varepsilon})$ of the investigated organic NLO materials were calculated using Eq. 8 and are tabulated in Table 9. Figure 9 illustrates the direct relationship between $(\boldsymbol{\varepsilon})$ and photon energy for all samples. As evident from the plot, the values of $(\boldsymbol{\varepsilon})$ exhibit a sharp decrease at low energy levels, followed by a nearly constant trend at higher gamma-ray energies [9]. This profile is a natural physical outcome of the transition from photoelectric absorption dominance at lower energies to Compton scattering dominance at higher energies. Overall, the comparison shows slightly higher $\%\Delta_2$ and $\%\Delta_3$ values for $C_{13}H_{11}N_3O_2$, which can be associated with its different elemental composition and corresponding elemental weight fractions. Furthermore, all modeling tools (Geant4, EpiXS, XCOM, and Phy-X/PSD) show good agreement, demonstrating a consistent trend among the simulated and theoretical datasets.

Table 9. Molar extinction coefficients and corresponding percentage deviations between the Geant4 results and the three theoretical tools for the $C_{17}H_{14}N_2O_2$ and $C_{13}H_{11}N_3O_2$ organic NLO compounds over the selected gamma-ray energy range.

Gamma Energy (MeV)	Molar extinction coefficients (ε (cm^2/mol))													
	$C_{17}H_{14}N_2O_2$							$C_{13}H_{11}N_3O_2$						
	Geant4	EpiXS	$\%\Delta_1$	XCOM	$\%\Delta_2$	Phy-X/PSD	$\%\Delta_3$	Geant4	EpiXS	$\%\Delta_1$	XCOM	$\%\Delta_2$	Phy-X/PSD	$\%\Delta_3$
0.1	0.550	0.550	0.010	0.550	0.031	0.5500	0.032	0.574	0.574	0.036	0.574	0.017	0.574	0.013
0.15	0.489	0.489	0.004	0.489	0.035	0.4889	0.041	0.509	0.509	0.037	0.510	0.113	0.510	0.085
0.2	0.446	0.446	0.007	0.446	0.008	0.4462	0.041	0.464	0.465	0.059	0.465	0.086	0.465	0.093
0.3	0.387	0.387	0.090	0.387	0.125	0.3870	0.127	0.403	0.403	0.052	0.403	0.069	0.403	0.089
0.4	0.346	0.346	0.067	0.347	0.170	0.3464	0.123	0.360	0.361	0.044	0.361	0.103	0.361	0.102
0.5	0.316	0.316	0.017	0.316	0.097	0.3162	0.092	0.329	0.329	0.023	0.329	0.103	0.329	0.097
0.6	0.292	0.292	0.128	0.292	0.184	0.2924	0.186	0.304	0.304	0.100	0.305	0.158	0.305	0.158
0.8	0.257	0.257	0.039	0.257	0.105	0.2567	0.103	0.267	0.267	0.005	0.267	0.067	0.267	0.071
1	0.231	0.231	0.009	0.231	0.114	0.2308	0.109	0.240	0.240	0.040	0.240	0.135	0.240	0.140
1.5	0.187	0.188	0.096	0.188	0.250	0.1879	0.245	0.195	0.195	0.112	0.196	0.262	0.196	0.257
2	0.161	0.161	0.020	0.161	0.204	0.1612	0.193	0.168	0.168	0.030	0.168	0.209	0.168	0.205
3	0.129	0.129	0.099	0.129	0.273	0.1292	0.282	0.134	0.134	0.102	0.135	0.279	0.135	0.286
4	0.110	0.110	0.077	0.110	0.310	0.1104	0.306	0.115	0.115	0.044	0.115	0.286	0.115	0.274
5	0.098	0.098	0.056	0.098	0.293	0.0981	0.302	0.102	0.102	0.025	0.102	0.276	0.102	0.271
6	0.089	0.089	0.020	0.089	0.298	0.0893	0.279	0.093	0.093	0.060	0.093	0.302	0.093	0.319

7	0.083	0.083	0.022	0.083	0.296	0.0828	0.286	0.086	0.086	0.028	0.087	0.355	0.087	0.336
8	0.078	0.078	0.033	0.078	0.218	0.0778	0.221	0.081	0.081	0.033	0.081	0.311	0.081	0.286
9	0.074	0.074	0.090	0.074	0.178	0.0739	0.177	0.077	0.077	0.113	0.077	0.393	0.077	0.379
10	0.071	0.071	0.020	0.071	0.225	0.0707	0.244	0.074	0.074	0.015	0.074	0.264	0.074	0.278
11	0.068	0.068	0.036	0.068	0.289	0.0681	0.268	0.071	0.071	0.013	0.071	0.314	0.071	0.290
12	0.066	0.066	0.029	0.066	0.294	0.0659	0.295	0.069	0.069	0.061	0.069	0.334	0.069	0.326
13	0.064	0.064	0.047	0.064	0.275	0.0640	0.285	0.067	0.067	0.052	0.067	0.296	0.067	0.291
14	0.062	0.062	0.042	0.063	0.343	0.0625	0.332	0.065	0.065	0.023	0.065	0.298	0.066	0.311
15	0.061	0.061	0.007	0.061	0.305	0.0611	0.284	0.064	0.064	0.040	0.064	0.327	0.064	0.314
16	0.060	0.060	0.085	0.060	0.179	0.0599	0.170	0.063	0.063	0.035	0.063	0.310	0.063	0.290
18	0.058	0.058	0.052	0.058	0.274	0.0580	0.300	0.061	0.061	0.069	0.061	0.295	0.061	0.317
20	0.056	0.056	0.009	0.057	0.269	0.0565	0.250	0.059	0.059	0.014	0.059	0.298	0.059	0.273

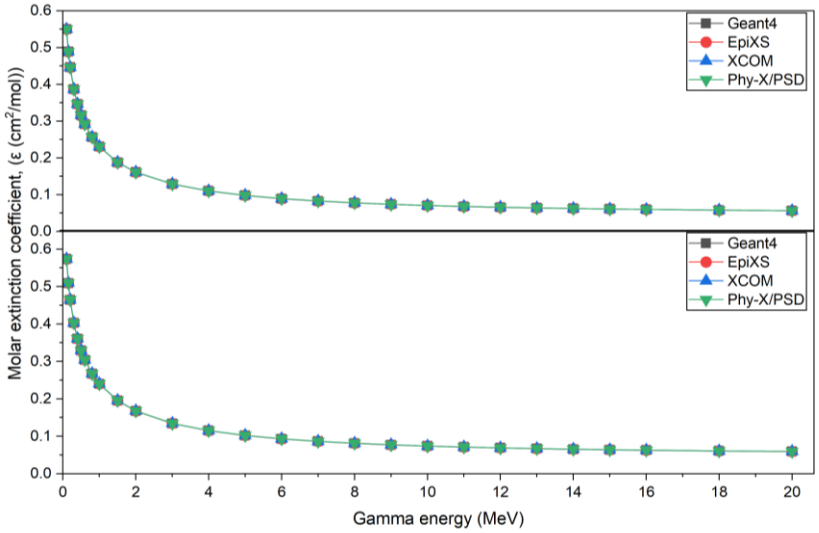


Fig.9. Comparative analysis of Geant4-simulated and theoretical molar extinction coefficients for (a) $C_{17}H_{14}N_2O_2$ and (b) $C_{13}H_{11}N_3O_2$ organic NLO compounds over the selected gamma energy range.

6. Conclusion

This work systematically evaluated the radiation shielding performance of organic non-linear optical (NLO) compounds across a broad energy range from 0.1 MeV to 20 MeV. Employing the Geant4 Monte Carlo toolkit alongside standard analytical frameworks, the gamma-ray attenuation parameters were rigorously determined to establish the overall shielding efficacy of the investigated materials. The simulation outcomes were compared with three established computational platforms (EpiXS, XCOM and Phy-X/PSD), showing good agreement with percentage deviations of less than 0.5% throughout the investigated range. For the first time, this study provides detailed information about (μ_m) values and other related parameters, such as $(\sigma_{t,a})$, $(\sigma_{t,el})$, (Z_{eff}), (N_{eff}) and $(\boldsymbol{\varepsilon})$ for two organic NLO compounds: 3-[1-(2-phenylhydrazinylidene)ethyl]-2H-chromen-2-one ($C_{17}H_{14}N_2O_2$) and 4-nitrophenyl hydrazone ($C_{13}H_{11}N_3O_2$). The obtained values of the mass attenuation coefficient (μ_m) coupled with the low effective atomic number (Z_{eff}) demonstrate the potential of the investigated organic NLO compounds in radiation therapy, diagnostic imaging and other technological applications. Total atomic and electronic cross-sections $(\sigma_{t,a}, \sigma_{t,el})$ exhibit an initial decrease as photon energy increases, similar to the mass attenuation coefficient (μ_m), and then become relatively independent of energy owing to the consecutive dominance of Compton scattering and pair production

within their respective energy ranges. The effective atomic numbers of the studied NLO samples were evaluated against various reference materials, including organic and inorganic NLO compounds, TLDs, polymers, and human tissues, showing close similarity, indicating that the investigated materials hold great potential for use in radiation dosimetry. Furthermore, the results indicate that Geant4 Monte Carlo simulations can serve as a useful computational tool for analyzing photon interactions with matter and for supporting comparative radiation-shielding studies.

Funding

The author declares that no funds, grants, or other support were received during the preparation of this manuscript.

Data Availability Statement

All data generated or analyzed during this study are included within the manuscript.

Conflicts of Interest

The author declares no conflict of interest.

References

[1] V.V. Awasarmol, D.K. Gaikwad, S.S. Obaid, P.P. Pawar, Gamma radiation studies on organic nonlinear optical materials in the energy range 122–1330 keV, Proc. Natl. Acad. Sci., India, Sect. A Phys. Sci. 90 (2020), pp. 839–844. https://doi.org/10.1007/s40010-019-00636-1

[2] M.R. Suresh Kumar, H.J. Ravindra, S.M. Dharmaprakash, Synthesis, crystal growth and characterization of glycine lithium sulphate. J. Cryst. Growth. 306 (2007), pp. 361–365. https://doi.org/10.1016/j.jcrysgro.2007.05.015

[3] D.S. Chemla, J. Zyss, Nonlinear optical properties of organic molecules and crystals, vol 1. Academic, Orland, 1987.

[4] V.V. Awasarmol, D.K. Gaikwad, S.D. Raut, P.P. Pawar, Gamma ray interaction studies of organic nonlinear optical materials in the energy range 122 keV–1330 keV, Results Phys. 7 (2017), pp. 272–279. http://dx.doi.org/10.1016/j.rinp.2016.12.017

[5] V.V. Awasarmol, D.K. Gaikwad , S.D. Raut , P.P. Pawar, Photon interaction study of organic nonlinear optical materials in the energy range 122 keV to 1330 keV, Radiat. Phys. Chem. 130 (2017), pp.343-350. https://doi.org/10.1016/j.radphyschem.2016.09.012

[6] V.V. Awasarmol, P.P. Pawar, M.B. Solunke, Effective atomic numbers and effective electron densities of inorganic nonlinear optical materials in the energy range 356 keV -1330 keV, Int. J. Tech. Res. Sci. 2 (2017), pp.26-29.

[7] M.S. Al-Buriahi, V.P. Singh, Halil Arslan, V.V. Awasarmol, B.T. Tonguc, Gamma-ray attenuation properties of some NLO materials: potential use in dosimetry, Radiat. Environ. Biophys. 59 (2020), pp.145–150. https://doi.org/10.1007/s00411-019-00824-y

[8] S. Bhadauria, M. Das, S. Saxena, R. Prasad, P. Sen, R. Dwivedi, Recent progress in non-linear optical material, syntheses, characterization and geometry optimization of dicinnamalacetone. Arch. Phys. Res. 2 (2011), pp.36–44.

[9] Vishal Vishwanath Awasarmol, Gamma ray attenuation parameters of inorganic nonlinear optical materials in the energy range 122 keV to 1330 keV, Indian J. Pure Appl. Phys. 55 (2017), pp. 65-72.

[10] H. Baltas, S. Celik, U. Cevik, E. Yamaz, Measurements of mass attenuation coefficient and effective atomic number for MgB2 superconductor using X-ray energies, Radiat. Meas. 42 (2007), pp.55–60. https://doi.org/10.1016/j.radmeas.2006.08.005

[11] S.S. Shaikh, S.B. Borul, S.S. Khan, A study on the gamma-ray attenuation coefficient parameters for potassium carbonate, Int. J. Eng. Technol. Manag. Sci. 7 (2023), pp.79-86. https://doi.org/10.46647/ijetms.2023.v07i03.011

[12] Z. Aygün, M. Aygün, Radiation shielding potentials of $Hf_{0.5}Mo_{0.5}NbTiZrCrx$ (X=0.1,0.3,0.5) refractory high entropy alloys by EPIXS, Rahva J. Tech. Soc. Stud. 3 (2023), pp. 83-95.

[13] Z. Aygun, Study on radiation shielding characteristics of refractory high entropy alloys by EpiXS code, Acta Phys. Pol. A, 143 (2023), pp.66-74. https://doi.org/10.12693/APhysPolA.143.66

[14] V.P. Singh, S.P. Shirmardi, M.E. Medhat, N.M. Badiger, Determination of mass attenuation coefficient for some polymers using Monte Carlo simulation, Vacuum, 119 (2015), pp. 284-288. https://doi.org/10.1016/j.vacuum.2015.06.006

[15] C.V. More, H. Alavian , P.P. Pawar, Evaluation of gamma-ray attenuation characteristics of some thermoplastic polymers: Experimental, WinXCom and MCNPX studies, J. Non-Cryst. Solids, 546 (2020), https://doi.org/10.1016/j.jnoncrysol.2020.120277

[16] G.A. Urfa, T. Wianto, T.N. Manik, A.V. Nasrulloh, Study of alternative shielding material for gamma radiation using Monte Carlo simulation, J. Teknol. Reaktor Nuklir, 25 (2023), pp. 101–106. https://doi.org/ 10.55981/tdm.2023.6925

[17] I. Han, L. Demir, Mass attenuation coefficient, effective atomic and electron number of Ti and Ni alloy, Radiat. Meas. 44 (2009), PP.289–294. https://doi.org/10.1016/j.radmeas.2009.03.010

[18] I. Han, L. Demir, M. Sahin, Determination of mass attenuation coefficient, effective atomic number and electron number for some natural minerals. Radiat. Phys. Chem. 78 (2009), pp. 760–764. https://doi.org/10.1016/j.radphyschem.2009.03.077

[19] M.E. Medhat, V.P. Singh, Mass attenuation coefficients of composite materials by Geant4, XCOM and experimental data: comparative study. Radiat. Eff. Defects Solids, 169 (2014), pp. 800–807. http://dx.doi.org/10.1080/10420150.2014.950264

[20] K. Alsafi , D. Abdullah Aloraini , H.M. Almutairi , S.A.M. Issa , H.M.H. Zakaly, K.S. Shaaban, Comprehensive study of optical, thermal, and gamma-ray shielding properties of B_2O_3–SiO_2–BeO–MgO–La_2O_3, glasses, Opt. Mater. 150 (2024). https://doi.org/10.1016/j.optmat.2024.115298

[21] H.A. Ali , I.I. Turki , G.Sh. Al-Obaidy , J.M. Rzaij, Evaluating the gamma-ray attenuation characteristics of various radioactive sources using binary and ternary polymer blends, J. Compos. Adv. Mater. 35 (2025), pp. 935-945. https://doi.org/10.18280/rcma.350513

[22] S.G. Uzun1, H. Eroğlu, B. Bilmez, M.Ç. Tufan, M. Gürbüz, B.C. Turan, Gamma attenuation properties of $SrTiO_3$ doped with Rb and Y, Cumhuriyet Sci. J., 46 (2025), pp. 949-956. https://doi.org/10.17776/csj.1739508

[23] Z.A. Alrowaili, E.O. Echeweozo, S. Alomairy, A. Hammoud, C. Sriwunkum, N.S. Alsaiari, I. Boukhris , M.S. Al-Buriahi, Gamma attenuation, buildup factors, and radiation shielding performance of CaO-borosilicate glasses , J. Radiat. Res. Appl. Sci. 18 (2025). https://doi.org/10.1016/j.jrras.2024.101221

[24] M.W. Aladailah, M.W. Marashdeh, H. Akhdar , O.L. Tashlykov, Al-Tamimi Walaa and A.A. Ghazal, Investigation of the gamma and neutron radiation properties of strontium bismuth borate glasses doped with neodymium ions using the Geant4 simulation toolkit and EpiXS software, Radiat. Eff. Defects Solids, 178 (2023), pp. 485–499. https://doi.org/10.1080/10420150.2022.2153250

[25] M.I. Sayyed, O.I. Olarinoye, M. Elsafi, Assessment of gamma-radiation attenuation characteristics of Bi_2O_3–B_2O_3–SiO_2–Na_2O glasses using Geant4 simulation code, Eur. Phys. J. Plus, 136 (2021). https://doi.org/10.1140/epjp/s13360-021-01492-y

[26] A.A. SKIN, Evaluation of the gamma and neutron shielding properties of $64TeO_2 + 15ZnO + (20 - x)CdO + xBaO + 1V_2O_5$ glass system using Geant4 simulation and Phy-X database software, Pramana – J. Phys. 94 (2020). https://doi.org/10.1007/s12043-020-01972-3

[27] F.H. Alkallas, A.G. Trabelsi, S. Elaissi, T.A. Alrebdi, L. Abu El Maati, F. B. M. Ahmed, M. M. Mahasen, M. Ahmad, M. M. Soraya, Investigation of the gamma photon shielding in Se–Te–Ag chalcogenide glasses using the Phy-X/ PSD software, Cogent Eng. 9 (2022). https://doi.org/10.1080/23311916.2022.2116829

[28] H. Akhdar, Theoretical investigation of gamma- and neutron-shielding properties of polysulfone (PSU) polymer material using Geant4, Polymers, 14 (2022). https://doi.org/10.3390/polym14163374

[29] R.R. Bhosale, C.V. More, D.K. Gaikwad, P.P. Pawar, M.N. Rode, Radiation shielding and gamma ray attenuation properties of some polymers, Nucl. Technol. Radiat. Prot. 32 (2017), pp. 288-293. http://doi.org/10.2298/NTRP1703288B

[30] S.R. Manohara, S.M. Hanagodimath, L. Gerward, The effective atomic numbers of some biomolecules calculated by two methods: A comparative study, Med. Phys., Vol. 36 (2009), pp.137-141. https://doi.org/10.1118/1.3030952

[31] V. Zebardast, A.A. Saray, Experimental and simulation study of shielding features of polyester/ HgO composites against photons using GEANT4 and MCNP codes, Sci. Rep. 15 (2025). https://doi.org/10.1038/s41598-025-17942-x

[32] J.H. Hubbell, S.M. Seltzer, Tables of X-ray mass attenuation coefficients and mass energy absorption coefficients 1 keV to 20 MeV for elements Z = 1 to 92 and 48 additional substances of dosimetric interest. Natl. Inst. Stand. Phys. Lab, NISTIR; (1995). https://dx.doi.org/10.18434/T4D01F

[33] J.H. Hubbell, Photon mass attenuation and energy absorption coefficients. Int. J. Appl. Radiat. Isot. 33 (1982). pp.1269–1290. https://doi.org/10.1016/0020-708X(82)90248-4

[34] M.J. Berger, J.H. Hubbell, (XCOM) Photon cross section on a personal computer. National Bureau of Standards, Gaithersburg, MD, NBSIR 87-3597, Jul. 1987.

[35] L. Gerward, N. Guilbert, K.B. Jensen, H. Levring, X-ray absorption in matter, reengineering XCOM, Radiat. Phys. Chem. 60 (2001), pp. 23–24. https://doi.org/10.1016/S0969-806X(00)00324-8

[36] T.K. Kumar, K.V. Reddy, Effective atomic numbers for materials of dosimetric interest. Radiat. Phys. Chem. 50 (1997), pp. 545-553. https://doi.org/10.1016/S0969-806X(97)00089-3

[37] C.T. Chantler, Theoretical form factor, attenuation, and scattering tabulation for Z = 1–92 from E = 1–10 eV to E = 0.4–1.0 MeV. J. Phys. Chem. Ref. Data, 24 (1995), pp. 71- 643. https://doi.org/10.1063/1.555974

[38] Shivaramu, V. Ramprasath, Effective atomic numbers for photon energy absorption and energy dependence of some thermoluminescent dosimetric compounds. Nucl. Instrum. Methods Phys. Res., Sect. B, 168 (2000), pp. 294-304. https://doi.org/10.1016/S0168-583X(99)01100-3

[39] S. Gowda, S. Krishnaveni, T. Yashoda, T.K. Umesh, R. Gowda, Photon mass attenuation coefficients, effective atomic numbers and electron densities of some thermoluminescent dosimetric compounds. Pramana, 63 (2004), pp. 529-541. https://doi.org/10.1007/BF02704481

[40] S. Agostinelli, J. Allison, K. Amako, J. Apostolakis, H. Araujo, P. Arce, M. Asai, D. Axen, S. Banerjee, G. Barrand, et al. Geant4—A simulation toolkit. Nucl. Instrum. Methods Phys. Res., Sect. A, 506 (2003), pp. 250–303. https://doi.org/10.1016/S0168-9002(03)01368-8

[41] C.T. Chantler, Detailed tabulation of atomic form factors, photoelectric absorption and scattering cross section, and mass attenuation coefficients in the vicinity of absorption edges in the soft X-ray (Z = 30–36, Z = 60–89, E = 0.1 keV–10 keV), addressing convergence issues of earlier work. J. Phys. Chem. Ref. Data, 29 (2000), pp. 597-801. https://doi.org/10.1063/1.1321055

[42] V.P. Singh, M.E. Medhat, N.M. Badiger, Photon attenuation coefficients of thermoluminescent dosimetric materials by Geant4 toolkit, XCOM program and experimental data: a comparison study. Ann. Nucl. Energy, 68 (2014), PP. 96-100. https://doi.org/10.1016/j.anucene.2014.01.011

[43] Shivaramu, Effective atomic numbers for photon energy absorption and photon attenuation of tissues from human organs. Med. Dosim. 27 (2002), PP.1-9. https://doi.org/10.1016/S0958-3947(01)00078-4

[44] Z-G. Yin, H-Y. Qian, J. Jia, N. Zhou, L-Q. Feng, (E)-1-Benzylidene-2-(4-nitrophenyl)hydrazine, Acta Crystallogr., Sect. E 62 (2006), pp. o4913–o4914. https://doi:10.1107/S1600536806040372